A ferromagnetic insulating substrate for the epitaxial growth of topological insulators

Huiwen Ji,[1] R. A. Stokes,[1] L. D. Alegria,[2] E. C. Blomberg,[3] M. A. Tanatar,[3] Anjan Reijnders,[4] L. M. Schoop,[1] Tian Liang,[2] R. Prozorov,[3] K. S. Burch,[4,5] N. P. Ong,[2] J. R. Petta,[2] and R. J. Cava[1]

[1]*Department of Chemistry, Princeton University, Princeton, New Jersey 08544, USA*
[2]*Department of Physics, Princeton University, Princeton, New Jersey 08544, USA*
[3]*Ames Laboratory and Department of Physics and Astronomy, Iowa State University, Ames, Iowa 50011, USA*
[4]*Department of Physics and Institute for Optical Sciences, University of Toronto, Toronto, Ontario M5S 1A7, Canada*
[5]*Department of Materials Science and Engineering, 170 College Street, Toronto, Ontario M53 3E4, Canada*

(Received 29 July 2013; accepted 9 September 2013; published online 20 September 2013)

$Cr_2Ge_2Te_6$ is proposed as an insulating ferromagnetic substrate for the growth of tetradymite-type topological insulators, based on a refined characterization of its transport, magnetic, optical, and calculated electronic properties. It is found to be a soft ferromagnet with no visible magnetic domains over relatively large length scales and to be highly insulating with an indirect band gap and low carrier concentration. Further we present the fabrication of Bi_2Te_3-$Cr_2Ge_2Te_6$ heterostructure samples by chemical vapor deposition and show that crystals of the two phases are oriented such that the hexagonal Te planes are aligned at their interfaces. © *2013 AIP Publishing LLC*. [http://dx.doi.org/10.1063/1.4822092]

INTRODUCTION

Topological insulators (TIs) have recently emerged as an active topic of research in condensed matter physics, motivating the further development of the concept of topology in materials studies.[1–5] It is known that the unconventional conducting surface states on 3D TIs are protected by time-reversal (TR) symmetry.[6] Through breaking the TR symmetry as a result of the presence of ordered magnetic moments in bulk of a 3D TI, a new phenomenon called the quantum anomalous Hall effect (with quantized Hall conductance in the absence of an external magnetic field) may be observed.[7] A primary obstacle to realizing this prediction is the difficulty in obtaining homogeneous magnetically doped TIs.[8] There have also been numerous proposals to use TI surface states as a platform for topological quantum computation. These proposals require placing the TIs in intimate contact with a ferromagnetic insulator,[9,10] and recently an alternative strategy has been suggested[11] to achieve this goal by depositing a layer of heavy atoms with large spin-orbit coupling on a magnetically ordered insulating substrate. These proposals involving a ferromagnetic insulator would avoid the aforementioned problem of incorporating the TI surface states and the ferromagnetism in the same material.

We propose that lamellar materials of the magnetic 3*d* transition elements can be ideal candidates for substrates due to their layered structures and localized magnetic moments. Among these materials, single crystals of $Cr_2Ge_2Te_6$ have been synthesized and are known to display a ferromagnetic transition at 61(±1) K.[12] Further, this compound is one of a handful of known ferromagnetic insulators. The pattern of the topmost Te surface layer upon cleaving $Cr_2Ge_2Te_6$ follows the same basic hexagonal geometry array as that found in the tetradymite family of TIs (such as Bi_2Te_3 (Ref. 13)), making $Cr_2Ge_2Te_6$ a natural fit as a substrate for epitaxial growth of members of the currently most studied TIs.

In this report, we reinvestigate the crystal structure of crystals of $Cr_2Ge_2Te_6$ grown from flux and refine the understanding of its magnetic, optical, and transport properties. Our magnetization and magneto-optical measurements indicate that $Cr_2Ge_2Te_6$ is an extremely soft ferromagnetic material with no detectable hysteresis (coercive field < 100 Oe). The saturation moment is $\sim 3\ \mu_B/Cr^{3+}$. Optical spectra reveal a band gap of ~ 0.74 eV. Electronic structure calculations show that the band gap is indirect and is a consequence of the strong Hund's rule coupling of Cr^{3+}. Finally, we report the growth of Bi_2Te_3 on a $Cr_2Ge_2Te_6$ substrate via metalorganic chemical vapor deposition (MOCVD). Bi_2Te_3 crystallizes in two morphologies on the substrates, as oriented triangular islands ($\sim 2\ \mu m \times 2\ \mu m$ in size) and continuous thin films ($\sim 400\ \mu m \times 400\ \mu m$ in size, ~ 100 nm in thickness). Electron Backscattered Diffraction (EBSD) reveals a consistent 30° rotation around the *c* axis of the unit cells of Bi_2Te_3 and $Cr_2Ge_2Te_6$, confirming that Bi_2Te_3 is epitaxially grown on the $Cr_2Ge_2Te_6$ substrate.

EXPERIMENTAL

To grow single crystals of $Cr_2Ge_2Te_6$, starting materials of high purity elemental Cr (99.99%), Ge (99.999%), and Te (99.999%) were employed, mixed in a molar ratio of 2:6:36; the extra Ge and Te were used as a flux.[12] The materials were heated to 700 °C, held for 20 days and then slow cooled to 500 °C over a period of 1.5 days. This was followed by centrifugation to remove the flux. The resultant platelet single crystals are a few millimeters in size and have a silvery luster. Before carrying out structural or property characterization, the samples were annealed in sealed evacuated quartz

tubes at ~400 °C in a horizontal tube furnace with a temperature gradient to remove the residual Te flux. The purity of the crystals was then investigated on a Bruker D8 Focus powder X-ray diffractometer operating with Cu Kα radiation and a graphite diffracted beam monochromator (PXRD). The single crystal X-ray diffraction study was conducted on a Bruker APEX II diffractometer using Mo Kα radiation.

Temperature-dependent resistivity and Hall measurements were carried out using a Quantum Design Physical Property Measurement System (PPMS). Silver paint was used to make contacts for both measurements. Magnetic susceptibilities and the temperature and field dependences of the magnetization were measured by using the PPMS. The Optical transmittance of $Cr_2Ge_2Te_6$ was measured at 292 K between 50 and 900 meV using a modified Bruker Vertex 80v FTIR spectrometer.

Magneto-optical imaging of the component of the magnetic induction perpendicular to the sample surface was conducted by utilizing the Faraday effect in bismuth-doped iron garnet ferrimagnetic films with in-plane magnetization.[14] When linearly polarized light passes through such a film and reflects off the mirror sputtered on its bottom, it picks up a double Faraday rotation proportional to the intensity of the magnetization along the light path, perpendicular to the indicator (and sample) surface. This component of magnetization is proportional to the perpendicular component of the magnetic induction at a given location on the sample surface. Observed through a linear analyzer at close to a 90° angle to the polarizer, a real-time 2D image is obtained where the intensity is proportional to the perpendicular component of the magnetic field on the sample surface.[14] For the low-temperature experiment, a flow-type liquid ^{4}He cryostat with the sample in vacuum was used. The sample was positioned on top of a copper cold finger, and an indicator film is placed on top of the sample. Spatial resolution was determined by several factors, mostly by the distance from the film to the sample surface, estimated to be about 2–4 μm. The cryostat was positioned under a polarized-light reflection, Leica DMLM, microscope, and the color images were recorded with high-resolution cooled CCD camera.

The electronic structure calculations were performed in the framework of density functional theory (DFT) using the WIEN2K (Ref. 15) code with a full-potential linearized augmented plane-wave and local orbitals [FPLAPW + lo] basis[16–18] together with the Perdew Burke Ernzerhof (PBE) parameterization[19] of the generalized gradient approximation (GGA) as the exchange-correlation functional. The plane wave cut-off parameter $R_{MT}K_{MAX}$ was set to 7, and the irreducible Brillouin zone was sampled by 300k-points. The lattice parameters and atomic positions obtained in this work were employed for the structural input.

Finally, a $Cr_2Ge_2Te_6$-Bi_2Te_3 heterostructure was grown by using MOCVD.[20,21] A single-crystal flake (~1 mm × 1 mm × 7 μm) of $Cr_2Ge_2Te_6$ was mechanically exfoliated as a substrate and stored in dry N_2 prior to growth. For Bi_2Te_3 growth, the substrate was heated to a growth temperature of 280 °C in a 600 sccm flow of H_2 at 100 Torr. Once the substrate reached the growth temperature, vapors of diisopropyl telluride (DiPTe) and trimethyl bismuth (TMBi) were introduced into the gas stream, resulting in precursor partial pressures of $P_{DiPTe} = 2.8 \times 10^{-5}$ Torr and $P_{TMBi} = 7 \times 10^{-6}$ Torr in the growth chamber. The precursors thermally decompose at the sample, producing atomic bismuth and tellurium for crystal growth. After 30 min, the TMBi flow was stopped, terminating growth, and the sample is cooled to 100 °C with continued DiPTe flow.

RESULTS AND DISCUSSION

The crystal structure of $Cr_2Ge_2Te_6$ is shown in Figure 1. The X-ray diffraction pattern (Figure 1) from the basal plane crystal surface of a $Cr_2Ge_2Te_6$ single crystal only shows (003*n*) reflections, which indicates that the *c* axis is perpendicular to the platelets. The details of the structural characterization, based on single crystal X-ray diffraction, are given in Table I. Te layers, following a hexagonal *ACAC* stacking sequence, form the vertices of layers of edge-sharing octahedra; half of the octahedra are left empty in layers to create a van der Waals gap. Within a filled layer of octahedra, instead of a random mixture of Cr and Ge, 1/3 of the octahedra are filled by Ge-Ge dimers while the other 2/3 are filled by Cr ions. As a result, the Cr ions within one layer form a honeycomb-like pattern. The space group of $Cr_2Ge_2Te_6$ is *R*-3, resolving ambiguities due to the presence of crystal twinning in an earlier report.[12]

The zero-field cooled (ZFC) magnetic susceptibilities (not shown), $\chi = M/H$, were measured between 10 and 300 K, in an applied field of 1500 Oe perpendicular ($H \parallel c$) to the crystal basal plane. By fitting the high-temperature region of the susceptibility to the Curie-Weiss law

$$\chi - \chi_0 = C/(T - \theta), \tag{1}$$

where θ was determined to be ~80 K, indicating that $Cr_2Ge_2Te_6$ has dominantly ferromagnetic interactions. The field-dependent isothermal magnetizations were measured at temperatures of 10, 30, 50, and 70 K, with an increasing field

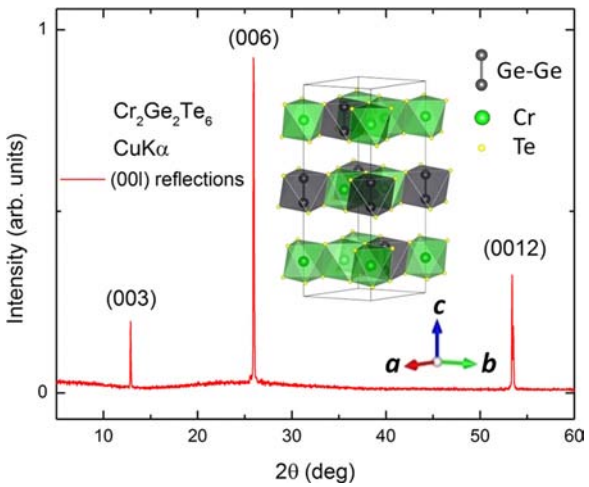

FIG. 1. The X-ray diffraction pattern from the basal plane crystal surface of $Cr_2Ge_2Te_6$ only shows (003 n) reflections, which indicates that the *c* axis is perpendicular to the platelets. The inset shows the crystal structure of $Cr_2Ge_2Te_6$, with Ge_2Te_6 and $CrTe_6$ octahedra colored gray and green, respectively. One third of the octahedra are filled by Ge-Ge dimers while the other 2/3 is filled by Cr ions.

TABLE I. Structural characterization of $Cr_2Ge_2Te_6$ (T = 300 ± 2 K). Space group *R*-3 (No. 148), *a* = 6.8286(4) Å, *c* = 20.5640(12) Å, 711 unique reflections, R_1 (all reflections) = 0.0271, wR_2 = 0.0392, twin domain proportions = 0.78896/0.21104, GooF (goodness of fit) = 1.099.

Atom	Wyck.[a]	x	y	z	U_{11}[b]	U_{22}[b]	U_{33}[b]	U_{12}[b]
Te	18f	0.33651(4)	0.29896(4)	0.082116(12)	0.01140(14)	0.01091(14)	0.01511(15)	0.00579(11)
Ge	6c	1/3	2/3	0.10874(3)	0.0105(2)	0.0105(2)	0.0189(4)	0.00524(10)
Cr	6c	0	0	0.16578(5)	0.0097(3)	0.0097(3)	0.0141(5)	0.00486(15)

[a]The Wyckoff position, a shorthand notation for atomic positions.
[b]Anisotropic displacement parameters, describing the atoms' thermal vibrations around their mean positions, in $Å^2$.

from −5 T to +5 T (shown in Figures 2(a) and 2(b)). The magnetizations exhibit a dramatic increase up to ∼5000 Oe for H // ab and ∼2500 Oe for H // c below the ferromagnetic transition temperature (T_c) of 61(±1) K.[12] Their saturated magnetization values reach ∼3 μB per Cr atom at 10 K, consistent with the expectation for high spin configuration state for Cr^{3+}. Here the *c* axis is the easy axis. The magnetization along the *c* axis saturates below 3000 Oe. The magnetization loop on varying the applied field from −5 to 5 T (Figure 2(c)) shows no measurable hysteresis to our level of precision, about 100 Oe, and a remnant magnetization is undetectable at the 100 Oe scale even at the low temperature of 5 K, indicating that $Cr_2Ge_2Te_6$ is an extremely soft ferromagnetic material.

Further and direct confirmation of the soft ferromagnetism is obtained by magneto-optical imaging. Figure 3(a) shows images recorded at 5 K in magnetic fields of 200, 400, and 600 Oe from left to right, respectively. The almost rectangular sample becomes clearly visible with a uniform intensity (proportional to the local magnetic field) much greater than the surroundings, indicating a magnetic induction much greater than the applied field, which is only possible in a ferromagnetic material. In fact, this image is similar to what is often obtained in soft ferromagnets such as transformer steel or various ferrites. The difference, however, is that in the case of $Cr_2Ge_2Te_6$ there is a large interval of magnetic fields where the magnetic induction is proportional to the applied field, indicating that the material has only moderate magnetic permeability; this is in contrast to the very high values found for soft steel, for example, which saturates its magnetization already in low, Oersted-level fields. Another significant observation for the current purposes is the apparent absence of ferromagnetic domains. Usually, this is associated with diminishing magnetocrystalline anisotropy[22] and indicates that the magnetic structure is such that the energy of formation for a domain wall is prohibitively high and the wall width is too large to serve the purpose of reducing the overall magnetostatic energy.

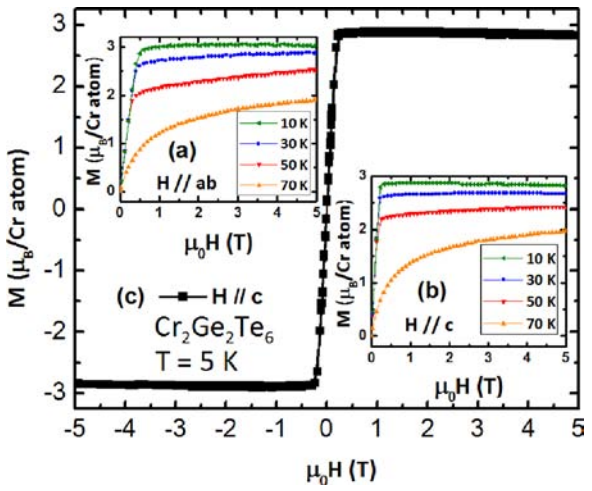

FIG. 2. (c) The magnetization with applied field perpendicular to the basal crystal surface from −5 to 5 T at 5 K. No magnetic hysteresis (coercive field < 100 Oe) was detected, indicating that $Cr_2Ge_2Te_6$ is a very soft ferromagnetic material. (a), (b) Insets show the field-dependent isothermal magnetizations measured at temperatures of 10, 30, 50, and 70 K, with the applied field parallel or perpendicular to the basal plane crystal surface.

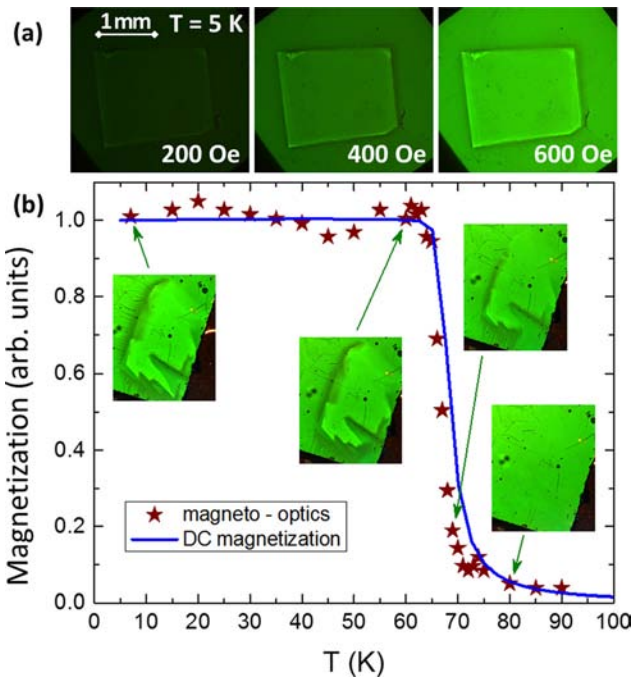

FIG. 3. (a) Magneto-optical images of an almost rectangular shaped single crystal of $Cr_2Ge_2Te_6$ at T = 5 K. There is a mirror between the sample surface and the indicator film, so all observed contrast comes solely from the magnetic field and not the physical shape of the sample, which is optically invisible. From left to right, the magnetic field was H = 200, 400, and 600 Oe, respectively. No ferromagnetic domains can be observed. (b) Temperature dependence of the normalized magnetization M(T)/M(0) (blue plot) and normalized intensity in the sample region (dark red stars). The good agreement between the two techniques indicates that $Cr_2Ge_2Te_6$ is a very soft ferromagnet without magnetic hysteresis. Four magneto-optical images are shown at different temperatures, and the intensity of the sample stands out below ferromagnetic transition temperature. Note that some images contain various "defects"—spots and streaks. These are optical artifacts due to dirt, grease, dust, and scratches on the substrate or mirror of the indicator films, and they do not affect the underlying imaging of magnetic fields in any way.

To confirm the ferromagnetism and compare the magneto-optical and magnetization measurements, the magnetic field intensity on the surface as a function of temperature while warming through the transition was measured (Figure 3(b)). The result, normalized to give 1 at T → 0 is shown in Figure 3(b). The results show very good agreement between the two techniques, which can only be the case for a very soft ferromagnet without magnetic hysteresis (or domains). The sample exhibits a clear transition temperature with temperature-independent behavior below the transition; these are characteristics of ferromagnetism.

Resistivity and Hall measurements were taken from room temperature down to low temperatures (26 K for resistivity and 60 K for Hall measurement) to characterize the electronic state of $Cr_2Ge_2Te_6$. Figure 4(b) shows a plot of resistivity vs. $1/T$; semiconducting behavior is shown. By linearly fitting the plot to the equation

$$\rho = \rho_0 \times \exp(E_a/2k_BT), \tag{2}$$

a transport energy gap (E_a) of ~202 meV was determined. The carrier type was found from Hall measurement to be p-type. Linearly fitting the plot of log carrier concentration (p) vs. $1/T$ (Figure 4(a)) within the high temperature region gives an energy gap of approximately 196 meV, which is consistent with that deduced from the resistivity measurement. We suggest that the p-type defects may dominate the system due to Ge vacancies

$$Ge_{Ge} \rightarrow V_{Ge}''' + 3h^{\bullet}, \tag{3}$$

the defect type suggested by first-principles study to have the lowest formation energy in the related compound rhombohedral GeTe.[18] The resistivity of $Cr_2Ge_2Te_6$ at 50 K is about $2.4 \times 10^4\ \Omega$ cm, and its carrier concentration at 60 K is about $2.1 \times 10^{14}\ cm^{-3}$ (the carrier concentration is too low to be detected below 60 K in our apparatus), indicating it to be a good insulator below its ferromagnetic transition temperature. At 300 K, the resistivity is about 0.46 Ω cm, and the carrier concentration is $8.3 \times 10^{16}\ cm^{-3}$. The IR transmission spectrum is presented in Figure 4(c). The data show a clear signature of Fabry-Pérot interference below 0.4 eV, indicative of high surface quality. Above 0.4 eV, two distinct absorption edges are observed, one at 0.5 eV and one at 0.74 eV. The origin of the absorption at 0.5 eV is not clear at this time, but the high-energy edge of transmittance (0.74 eV) unambiguously corresponds to an energy gap between valence and conduction bands.

The results of the calculation for the density of states and band structure of $Cr_2Ge_2Te_6$ are shown in Figure 5. Calculations were performed under the restricted ($\rho\uparrow = \rho\downarrow$) and unrestricted ($\rho\uparrow \neq \rho\downarrow$) spin formalisms; in the unrestricted case, the Cr was set as spin up. In the case where the spin up and spin down electron populations are constrained to be equal, we calculate a metallic band structure. The Fermi level in this case would be located at a high peak in the density of states (DOS), which belongs to Cr 3d states and can be attributed to the half-filled t_{2g} manifold. This is in agreement with previous calculations.[12] However, this electronic picture is inconsistent with the well known chemical character of t_{2g}^3 Cr^{3+} in octahedral coordination in insulators, which exhibits very strong Hund's rule coupling and consequently 3 unpaired electrons in the t_{2g} orbitals. This type of coupling is best described in electronic structure calculations through the use of unrestricted spin formalisms,

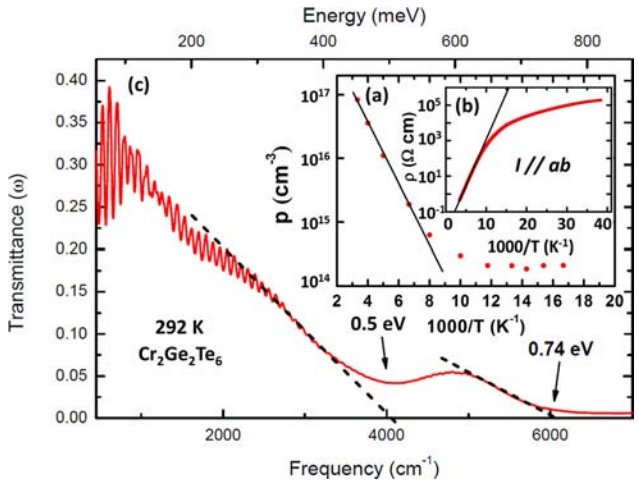

FIG. 4. (a) The linear fits of carrier concentration p and (b) resistivity ρ of $Cr_2Ge_2Te_6$. Both resistivity and Hall measurements were taken from room temperature down to low temperatures (26 K for resistivity and 60 K for Hall measurement). (c) The IR transmission spectrum of $Cr_2Ge_2Te_6$. Above 0.4 eV, two distinct absorption edges are observed at 0.5 eV and 0.74 eV, which are likely due to indirect bandgap transitions. The band gap is consistent with the high-wavenumber edge of transmittance, which is ~0.74 eV.

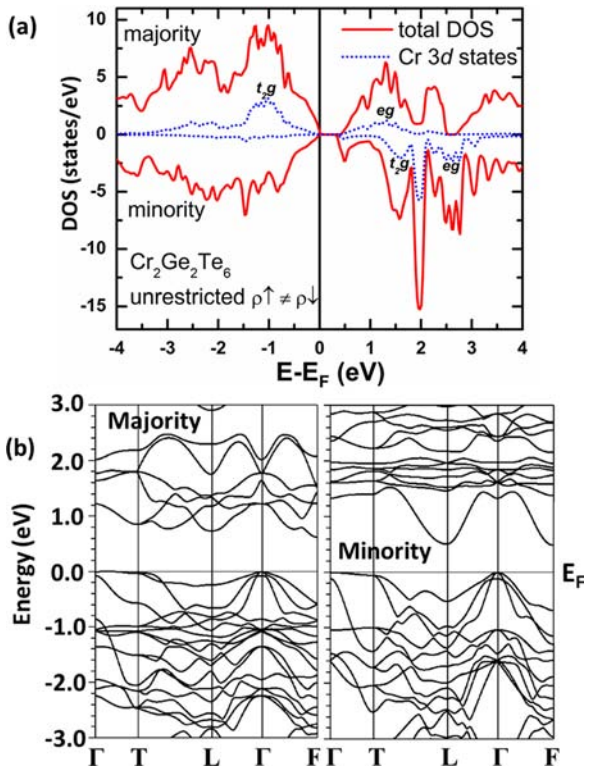

FIG. 5. (a) Calculated electronic density of states of $Cr_2Ge_2Te_6$ in the unrestricted spin formalism, allowing for Hund's rule coupling. A gap is visible in both spin channels. The Cr t_{2g} and e_g orbitals are indicated. (b) Band structures of $Cr_2Ge_2Te_6$ for the majority (left) and minority (right) spin channels. The band gap is indirect, between Γ and L in the minority spin channel.

where the spin up and spin down populations are allowed to vary independently. The Hund's rule coupling is a single-ion effect and does not depend on the presence of long range magnetic ordering in the material. Using this formalism for the $Cr_2Ge_2Te_6$ band structure calculation results in a band gap in both the majority and the minority spin channels (Figure 5(a)). This is the chemically reasonable electronic state of the system, and further comparison of the total energies between two models shows that the energy of the unrestricted, Hund's rule consistent spin formalism is 2.84 eV lower per formula unit, which strongly supports it as the more accurate way to describe the system.

The electronic structure calculations (Figure 5(b)) reveal that the band gap is indirect, between the Γ (valence band) and the L and F points (conduction band) in the minority spin channel. The predicted size of the indirect band gap between the valence band and minority spin channel in the conduction band, 0.43 eV, corresponds with one of the edges observed in the optical transmission experiments, as does the 0.7 eV gap in the majority spin channel. Further work would be required, however, to conclusively associate features in the optical spectra with those in the calculation.

The magnetic moment is calculated to be 3 μ_B per Cr atom, which is in good agreement with the expectations for a Cr^{3+} state as well as with the experimental results. Figure 5(a) shows the total DOS as well as the contribution from the Cr 3*d* states to both spin channels. The majority spins have a filled t_{2g} manifold and an empty e_g manifold, whereas both t_{2g} and e_g manifolds are empty for the minority spins, which also agrees with the expectations for Cr^{3+} ions in an octahedral geometry. Therefore, the insulating character of $Cr_2Ge_2Te_6$ is merely a natural consequence of the strong Hund's rule coupling of Cr^{3+}, and this material is not a Mott insulator.

$Cr_2Ge_2Te_6$ is reasonably closely lattice matched to the two most heavily studied topological insulator materials, Bi_2Se_3 (mismatch 4.8%)[23] and Bi_2Te_3 (mismatch 10.3%).[24] This fact is promising for the prospect of creating a topological insulator-ferromagnetic insulator junction, a long-standing goal of research in the field of topological insulator materials.[25] Although Bi_2Te_3 does not exhibit the mid-gap Dirac point that draws most attention to Bi_2Se_3, several practical advantages have led to the intensive study of Bi_2Te_3 TI surface states in various contexts.[26] In the present case of CVD growth on $Cr_2Ge_2Te_6$, an advantage is that the precursor DiPTe can be used for Bi_2Te_3 deposition. DiPTe pyrolyzes at sufficiently low temperatures that the substrate is well preserved, which is not true of the major Se precursors.[27] Using this method, we have created high quality $Cr_2Ge_2Te_6$-Bi_2Te_3 heterostructures.

After MOCVD deposition of Bi_2Te_3, crystallographically oriented triangular islands covered a large portion of the $Cr_2Ge_2Te_6$ substrate, with the rest remaining smooth. On inspection within a scanning electron microscope (SEM), the flat islands were observed to have dimensions on the scale 2 μm × 2 μm × 50 nm (Figure 6(a)). To study their composition, energy dispersive spectroscopy (EDS) was performed locally, on and off numerous islands. With the beam focused on the substrate, a composition of 21.0% Cr, 16.9% Ge, and 61.8% Te (mol. %) was measured, consistent with the expected composition of $Cr_2Ge_2Te_6$ and the few percent error characteristic of the technique. On the other hand, when focused on an island the electron beam generates X-rays both in the island and in the underlying substrate. In this case, a composition of 27.4% Bi, 61.6% Te, 5.8% Cr, and 5.2% Ge (mol. %) was detected, i.e., close to a $Bi_2Te_3 + Cr_2Ge_2Te_6$ composition. On the continuous deposited film, the EDS signature was similar to that observed on

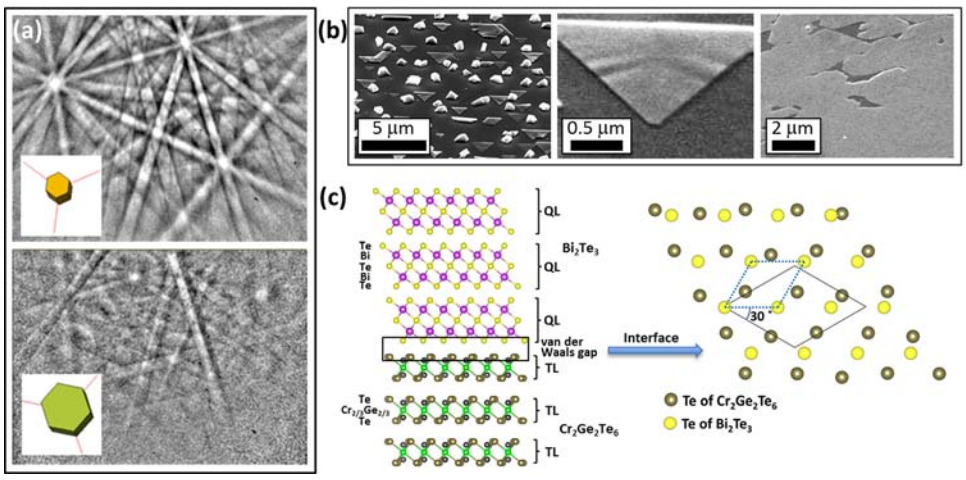

FIG. 6. Heteroepitaxy of Bi_2Te_3 on $Cr_2Ge_2Te_6$. (a) Electron backscatter diffraction patterns generated from spots ~100 nm in size on the triangular islands (top) and away from the islands (bottom) were indexed to the structures of Bi_2Te_3 on $Cr_2Ge_2Te_6$, respectively, with a relative rotation of the unit cells by 30° around their *c* axes. (b) SEM inspection at a 60° viewing angle. (left) A uniform growth of aligned triangular islands formed on the $Cr_2Ge_2Te_6$ surface, interspersed with pyramidal structures. EDS confirmed both species to be Bi_2Te_3. (center) Some islands show evidence of strain relaxation, likely due to the non-zero lattice mismatch. (right) About 30% of the substrate was covered with a continuous single crystalline Bi_2Te_3 film (~400 μm × 400 μm in size). (c) (left) The crystal structure of the Bi_2Te_3-$Cr_2Ge_2Te_6$ heterostructure. Each compound is displayed by one cell-edge length along its c axis. The quintuple Te-Bi-Te-Bi-Te layer in Bi_2Te_3 and the triple Te-($Cr_{2/3}$/$Ge_{2/3}$)-Te layer in $Cr_2Ge_2Te_6$ are labeled as QL and TL, respectively. There is a van der Waals gap between the two compounds. (right) A 30° rotation of the unit cells aligns the interfacial Te layers of the two crystals. The unit cells of $Cr_2Ge_2Te_6$ and Bi_2Te_3 are outlined by black solid lines and blue dotted lines, respectively. A high degree of ordering was observed, despite the lattice mismatch and the distortion of the geometry of the Te plane in $Cr_2Ge_2Te_6$.

the islands, implying that a continuous Bi_2Te_3 film grew in this region ($\sim$400 μm $\times$ 400 μm in size, $\sim$100 nm in thickness) as large islands merged together (Figure 6(a) right).

To structurally characterize the heterostructure, local EBSD was performed separately on the Bi_2Te_3 islands and the adjacent $Cr_2Ge_2Te_6$ substrate regions. Automatic diffraction pattern indexing (Oxford Instruments Flamenco software) positively identified the Bi_2Te_3 and $Cr_2Ge_2Te_6$ structures of islands and substrate, respectively, as shown in Figure 6(a). Further, the crystallographic orientations were directly compared in several pairs of substrate/island diffraction patterns. The pairs of unit cells had an average rotational offset of 29.9° $\pm$ 0.7° around the *c*-axis, with *c*-axes parallel within 0.1° $\pm$ 0.4°. In the region of the substrate with a continuous film, very similar Bi_2Te_3 EBSD patterns were collected at numerous points, showing the film ($\sim$30% of the substrate area) to be continuous single crystalline Bi_2Te_3.

Both Bi_2Te_3 and $Cr_2Ge_2Te_6$ are layered compounds. In Bi_2Te_3, the fundamental building block is a sandwich of five atomic layers (a quintuple layer, "QL"), Te-Bi-Te-Bi-Te, while in $Cr_2Ge_2Te_6$, the fundamental building block is three atomic layers (a triple layer, "TL"), Te-($Cr_{2/3}$/$Ge_{2/3}$)-Te. Each building block is charge balanced, and there are van der Waals gaps between them. The crystal growth of compounds of this type follows in a block-by-block fashion, and crystal cleavage always happens at the van der Waals Gaps. Therefore the exposed atomic layer of the $Cr_2Ge_2Te_6$ substrate is a Te atomic layer. The same argument holds for the deposited Bi_2Te_3, where the first layer has to be Te, as is also dictated by charge balance at the interface. Thus the proposed $Cr_2Ge_2Te_6$-Bi_2Te_3 interface, although not quantitatively characterized at the atomic level in this study, must be as shown in Figure 6(c) left.

The 30° rotation observed in EBSD is consistent with the alignment of the hexagonal lattices at the interfacial Te planes between Bi_2Te_3 and $Cr_2Ge_2Te_6$ (Figure 6(c) right).Despite the lattice mismatch, it is clear that Bi_2Te_3 is epitaxially grown on top of $Cr_2Ge_2Te_6$; this can be attributed to the flexible character of the van der Waals bonding between the Bi_2Te_3 layer and the $Cr_2Ge_2Te_6$ substrate. Nevertheless, there appeared to be some evidence of strain relaxation at the interface, as corrugation features can be observed in some of the Bi_2Te_3 islands (Figure 6(b) center). We expect that the highest quality films will eventually be obtained in future growth of Bi_2Se_3 films on the $Cr_2Ge_2Te_6$ surface, due to the reduced lattice mismatch.

CONCLUSION

In summary, the crystal structure and physical properties of the layered ferromagnetic insulator $Cr_2Ge_2Te_6$ were reinvestigated. The material is highly insulating and has a ferromagnetic T_c of 61 K. No magnetic hysteresis was detected within the sensitivity of our magnetization measurements, indicating that $Cr_2Ge_2Te_6$ is an extremely soft ferromagnetic material. This conclusion is confirmed by direct magneto-optical imaging that shows uniformly magnetized samples without resolvable ferromagnetic domains, behavior similar to that displayed by soft ferrites, with, however, the lower magnetic permeability resulting in much larger saturation fields for the current material. Combining the optical transmittance spectra and electronic structure calculations indicates an indirect band gap of $\sim$0.74 eV, while the small energy gap of $\sim$196–202 meV detected by transport measurements suggests the existence of *p*-type defect states. Finally, high quality Bi_2Te_3 was grown in two forms via MOCVD on $Cr_2Ge_2Te_6$-oriented triangular islands and continuous thin film. EBSD reveals a 30° rotational offset around the *c* axis between the unit cells of Bi_2Te_3 and $Cr_2Ge_2Te_6$, confirming that Bi_2Te_3 is epitaxially grown on top of $Cr_2Ge_2Te_6$ with the hexagonal Te planes at the interface in good registry.

We propose that by further optimizing growth conditions, larger continuous thin films of Bi_2Te_3 can be achieved on $Cr_2Ge_2Te_6$ to facilitate device fabrication and fundamental studies that require large material surfaces such as angle resolved photoemission spectroscopy (ARPES). In addition, this successful heterostructure growth of a tetradymite type compound on the insulating ferromagnet $Cr_2Ge_2Te_6$ serves as a model system for numerous variations, such as BiTeI(001)-$Cr_2Ge_2Te_6$, Bi_2Se_3(001)-$Cr_2Ge_2Te_6$, and SnTe(111)-$Cr_2Ge_2Te_6$, or simply depositing heavy elements such as elemental Bi on $Cr_2Ge_2Te_6$, providing a platform for studying the interaction between topological surface states or Rashba split states and ferromagnetism. The fact that the magnetization along the *c* axis saturates below 3000 Oe in $Cr_2Ge_2Te_6$ ensures that any interesting properties that may be displayed by this heterostructure can be observed with a low field.

ACKNOWLEDGMENTS

The research at Princeton University was supported by grants NSF DMR-0819860 and SPAWAR grant N66001-11-1-4110. The work in Toronto was funded by the Ontario Research Fund, the Natural Sciences and Engineering Research council of Canada, and the Canada Foundation for Innovation. A. A. Reijnders was supported by the Prins Bernhard Cultuurfonds. The work at Ames was supported by the U.S. Department of Energy, Office of Basic Energy Sciences, Division of Materials Sciences and Engineering under Contract No. DE-AC02-07CH11358.

[1]L. Fu and C. L. Kane, Phys. Rev. B **76**, 045302 (2007).
[2]Y. Xia, D. Qian, D. Hsieh, L. Wray, A. Pal, H. Lin, A. Bansil, D. Grauer, Y. S. Hor, R. J. Cava, and M. Z. Hasan, Nat. Phys. **5**, 398–402 (2009).
[3]J. Moore, Nat. Phys. **5**, 378–380 (2009).
[4]G. A. Fiete, Science **332**, 546–547 (2011).
[5]R. J. Cava, H. Ji, M. K. Fuccillo, Q. D. Gibson, and Y. S. Hor, J. Mater. Chem. C **1**, 3176–3189 (2013).
[6]C. L. Kane and E. J. Mele, Phys. Rev. Lett. **95**, 226801 (2005).
[7]F. D. M. Haldane, Phys. Rev. Lett. **61**, 2015–2018 (1988).
[8]H. Ji, J. M. Allred, N. Ni, J. Tao, M. Neupane, A. Wray, S. Xu, M. Z. Hasan, and R. J. Cava, Phys. Rev. B **85**, 165313 (2012).
[9]L. Fu and C. L. Kane, Phys. Rev. Lett. **102**, 216403 (2009).
[10]A. R. Akhmerov, J. Nilsson, and C. W. J. Beenakker, Phys. Rev. Lett. **102**, 216404 (2009).
[11]K. F. Garrity and D. Vanderbilt, Phys. Rev. Lett. **110**, 116802 (2013).
[12]V. Carteaux, D. Brunet, G. Ouvrard, and G. Andre, J. Phys.: Condens. Matter **7**, 69 (1995).
[13]Y. L. Chen, J. G. Analytis, J. H. Chu, Z. K. Liu, S. K. Mo, X. L. Qi, H. J. Zhang, D. H. Lu, X. Dai, Z. Fang, S. C. Zhang, I. R. Fisher, Z. Hussain, and Z. X. Shen, Science **325**, 178–181 (2009).

[14]C. Jooss, J. Albrecht, H. Kuhn, S. Leonhardt, and H. Kronmüller, Rep. Prog. Phys. **65**, 651 (2002).
[15]P. Blaha, K. Schwarz, G. K. H. Madsen, D. Kvasnicka, and J. Luitz, *An Augmented Plane Wave + Local Orbitals Program for Calculating Crystal Properties* (Techn. University at Wien, Wien, Austria, 2001).
[16]D. J. Singh and L. Nordström, *Planewaves, Pseudopotentials, and the LAPW Method* (Springer, New York, NY, 2006).
[17]G. K. H. Madsen, P. Blaha, K. Schwarz, E. Sjöstedt, and L. Nordström, Phys. Rev. B **64**, 195134 (2001).
[18]E. Sjöstedt, L. Nordström, and D. J. Singh, Solid State Commun. **114**, 15–20 (2000).
[19]J. P. Perdew, K. Burke, and M. Ernzerhof, Phys. Rev. Lett. **77**, 3865–3868 (1996).
[20]L. D. Alegria, M. D. Schroer, A. Chatterjee, G. R. Poirier, M. Pretko, S. K. Patel, and J. R. Petta, Nano Lett. **12**, 4711–4714 (2012).
[21]M. D. Schroer, S. Y. Xu, A. M. Bergman, and J. R. Petta, Rev. Sci. Instrum. **81**, 023903–023908 (2010).
[22]A. Hubert and R. Schäfer, *Magnetic Domains* (Springer-Verlag, Berlin, 2000).
[23]S. Nakajima, J. Phys. Chem. Solids **24**, 479–485 (1963).
[24]Y. Feutelais, B. Legendre, N. Rodier, and V. Agafonov, Mater. Res. Bull. **28**, 591–596 (1993).
[25]X.-L. Qi, R. Li, J. Zang, and S.-C. Zhang, Science **323**, 1184–1187 (2009).
[26]F. Xiu, L. He, Y. Wang, L. Cheng, L.-T. Chang, M. Lang, G. Huang, X. Kou, Y. Zhou, X. Jiang, Z. Chen, J. Zou, A. Shailos, and K. L. Wang, Nat. Nanotechnol. **6**, 216–221 (2011).
[27]M. Heuken, J. Cryst. Growth **146**, 570–579 (1995).